ADVANCED FUNCTIONAL MATERIALS
www.afm-journal.de

Multifunctional Eutectic Hydrogel with Antifreezing and Self-Powered Capabilities for Object Recognition Sensing

Zhongyang Cao, Chengfu Han, Yanlong Zhao, Ziteng Wang, Kangkang Zhou, Yajie Zhang, Wei Zhai, Guoqiang Zheng, Caofeng Pan,* Kun Dai,* Chuntai Liu, and Changyu Shen*

Hydrogels have attracted extensive research interest due to their remarkable stretchability and flexibility, enabling their integration into advanced applications such as flexible sensors, triboelectric nanogenerators (TENG), and supercapacitors. However, their high free water content renders them susceptible to freezing at subzero temperatures, leading to a loss of flexibility and severely restricting their performance in cold environments. To address this challenge, a freeze-resistant eutectic hydrogel composed of polyacrylamide (PAM)/deep eutectic solvent (DES)/phytic acid (PA) (PDP) eutectic hydrogel is systematically fabricated by partially replacing the free water in conventional hydrogels with DES. PDP eutectic hydrogel exhibits a combination of excellent properties, including high transparency (93%), exceptional stretchability (up to 1934% strain), and a high gauge factor (GF = 8.20). Importantly, PDP eutectic hydrogel retains excellent flexibility and stable sensing performance under extremely low temperatures. Its high sensitivity enables precise, real-time monitoring of human motions in flexible sensor arrays, which supports the development of a deep learning-integrated system capable of capturing subtle grasping motions and distinguishing between objects of varying shapes. This work offers a novel strategy to address the intrinsic freezing limitations of conventional hydrogels, significantly expanding their potential for use in demanding and low-temperature environments.

1. Introduction

In recent years, wearable electronic devices have emerged as indispensable components of next-generation electronic systems, catalyzing significant advances across interdisciplinary domains such as flexible sensors, triboelectric nanogenerators (TENG), and advanced flexible energy storage technologies.[1–3] Among the materials enabling this progress, hydrogels with an inherent 3D crosslinked polymer network possess unique properties, including high ionic conductivity, stretchability, tunable mechanical performance, and biocompatibility.[4,5] This multifunctional characteristic stems from the network's ability to entrap ionic species while maintaining structural integrity, making them well-suited for diverse roles in wearable electronics, such as stretchable electrodes, transducers in human-machine interfaces, and robust sensor systems.[6–8] However, high free water content inherent to most hydrogels introduces critical limitations, including environmental instability and susceptibility to freezing at subzero temperatures, which degrade both mechanical flexibility and electrical performance.[9,10]

To engineer cold-tolerant hydrogels for extreme environments, researchers introduce organic solvents into hydrogel systems.[11] These organic solvents effectively improve their mechanical properties under extremely cold conditions.[12,13] However, the incorporation of organic solvents can compromise the electrical conductivity of hydrogels, and some organic solvents are associated with cytotoxicity or environmental hazards.[14,15] Compared to organic solvents, ionic liquids can not only improve the low-temperature stability of hydrogels but also enhance electrical conductivity through establishing ionic channels within the network.[16,17] However, their widespread application is hindered by high cost, complex synthesis procedures, and in many cases, inherent toxicity and environmental concerns. In contrast, eutectic hydrogels formulated with deep eutectic solvents (DES) offer a more sustainable and versatile alternative. DES is synthesized through strong hydrogen bonding interactions between hydrogen bond donors (HBDs) and hydrogen bond acceptors (HBAs)[18] and is recognized as green solvents with multiple advantages. These include simple manufacturing

Z. Cao, Y. Zhao, Z. Wang, K. Zhou, Y. Zhang, W. Zhai, G. Zheng, C. Pan, K. Dai, C. Liu, C. Shen
School of Materials Science and Engineering
Key Laboratory of Materials Processing and Mold (Zhengzhou University)
Ministry of Education
Zhengzhou University
Zhengzhou 450001, P. R. China
E-mail: weizhai@zzu.edu.cn; pancaofeng@buaa.edu.cn; kundai@zzu.edu.cn

C. Han
School of Electro-Mechanical Engineering
Zhongyuan Institute of Science and Technology Xuchang
Xuchang 461000, P. R. China

C. Pan
Institute of Atomic Manufacturing
Beihang University
Beijing 100191, P. R. China

The ORCID identification number(s) for the author(s) of this article can be found under https://doi.org/10.1002/adfm.202529024

DOI: 10.1002/adfm.202529024

processes, high cost-effectiveness,[19] good biocompatibility,[20] enhanced structural stability,[21] and excellent conductivity,[22] making them particularly ideal for utilization in TENGs and flexible electronic systems.[23–26] Therefore, DES-based hydrogels present new prospects for achieving sustainable, high-performance soft electronic devices capable of reliable operation under harsh, subzero conditions.[27,28]

DES contains diverse functional groups, which enable the formation of dense hydrogen bond networks with water molecules. Therefore, these interactions effectively convert free water into bound water within the hydrogel matrix, thereby imparting intrinsic antifreezing and water-retention capabilities to DES-based eutectic hydrogels.[29] Betaine (HBA) exhibits exceptional chemical robustness, resisting hydrolysis and oxidation while maintaining stability over wide pH ranges and elevated temperatures. Glycerol, acting as a highly active HBD, offers multiple proton-donating sites that engage in dense and cooperative hydrogen-bonding interactions with HBA. Such multivalent hydrogen-bonding coordination reinforces the intermolecular network, thereby markedly enhancing the stability of the eutectic system. Meanwhile, to further improve the electrical conductivity of eutectic hydrogels, phytic acid has been introduced as a functional additive.[30] Phytic acid (PA), a naturally occurring organic macromolecule, consists of an inositol ring covalently connected to six phosphate groups via phosphate ester linkages.[31–33] Upon ionization, the phosphate groups release protons, which significantly increase the ionic conductivity of the hydrogel. Simultaneously, intermolecular interactions mediated by the phosphate moieties reinforce the mechanical robustness of the gel network. Despite these advances, current DES formulations are primarily limited to combinations such as choline chloride (ChCl) and urea,[34,35] restricting the diversity and tunability of DES systems for hydrogel engineering. Therefore, the design and development of multifunctional DES-based hydrogels with integrated antifreezing properties, high mechanical flexibility, and broad environmental adaptability remains a critical objective in advancing the next generation of soft electronic materials.

In this study, a PAM-DES-PA (PDP) eutectic hydrogel was rationally synthesized via the formulation of DES with glycerol and betaine as components. Through molecular design optimization, the resulting PDP eutectic hydrogel exhibits a remarkably wide working range (1934% strain), high gauge factor (GF = 8.20), rapid response times (150 ms), and strong inherent adhesiveness. Integrating its intrinsic flexibility, high sensitivity, and robust ionic transport capability, the PDP eutectic hydrogel functions effectively as both flexible sensors for human motion monitoring and compliant electrodes for TENG. Notably, it retains mechanical integrity and strain sensing performance under extreme cryogenic conditions, enabling real-time tracking of human motion at subzero temperatures. Leveraging its multifunctional characteristics, we demonstrate the feasibility of a deep learning-assisted soft mechanical gripper for discriminative recognition of objects with diverse geometric configurations. This work not only advances the frontier of smart hydrogel materials but also offers a versatile strategy for developing next-generation wearable electronics and adaptive soft robotics for extreme environments.

2. Results and Discussion

2.1. Preparation of PDP Eutectic Hydrogel

The synthesis of PDP eutectic hydrogel is shown in **Figure 1a**. Glycerol (HBD) and betaine (HBA) are mixed at 80 °C for 2 h to form DES (Figure S1, Supporting Information). This process follows the simple and green principle, and no by-products are generated. PDP eutectic hydrogels are prepared through free-radical copolymerization of acrylamide (AM) and PA in the presence of DES and H_2O, with N, N'-methylene-bis-acrylamide (MBA) as the crosslinking agent and ammonium persulfate (APS) as the initiator (Figure S2, Supporting Information). Compared to conventional PAM hydrogels, the DES in PDP partially replaces free water, forming bound water through intermolecular interactions between DES and H_2O. This interaction suppresses ice crystallization at low temperatures, endowing the PDP eutectic hydrogel with cryotolerance and functionality in subzero environments (Figure 1b).[36–38] The molecular electrostatic potential energy surface analyses of DES, H_2O, and PA further highlight the strong intermolecular interactions that contribute to the PDP eutectic hydrogel's multifunctionality (Figure 1c). The DES and PA contained in the PDP eutectic hydrogel endow it with multifunctionality. Due to the synergistic incorporation of DES and PA, the PDP eutectic hydrogel exhibits broad application potential across various domains, including motion sensing, triboelectric energy harvesting, and machine learning-enabled intelligent systems (Figure 1d). In particular, we propose a TENG-based soft gripper platform utilizing PDP eutectic hydrogel for object shape recognition. By generating a dataset of shape-related signals, this platform enables machine learning classification based on geometric features, demonstrating the promise of intelligent soft robotic interaction.

2.2. Mechanical Properties and Characteristic of PDP Eutectic Hydrogel

To optimize the mechanical properties of the PDP eutectic hydrogel, the mass ratios of DES, PA, and H_2O are systematically investigated. The hydrogel is defined as PD_xP_y, where x and y denote the mass ratios of DES and PA in the hydrogel. The Young's modulus, toughness, fracture strain, and fracture stress of PDP eutectic hydrogel at the optimal ratio were analyzed in detail. As shown in **Figure 2a**, with the increasing DES content, the strain, stress, and modulus of the hydrogels first increased and then decreased (Figure S3, Supporting Information). The hydroxyl groups provided by DES act as physical crosslinkers in the hydrogel, forming intermolecular hydrogen bonds with PAM chains and water molecules to enhance the crosslinking density, thereby improving the mechanical properties. Similarly, the PA content also modulates the mechanical properties, as shown in Figure 2b,c. At low PA concentrations, the polyphosphate groups in PA participate in dynamic ionic crosslinking with polymer chains, which increases the effective crosslinking density and enhances both toughness and modulus. However, at high PA levels, excessive ionic crosslinking rigidifies the network structure and reduces stress tolerance due to restricted chain mobility. Rheological characterization of PDP eutectic hydrogel and PP hydrogel revealed

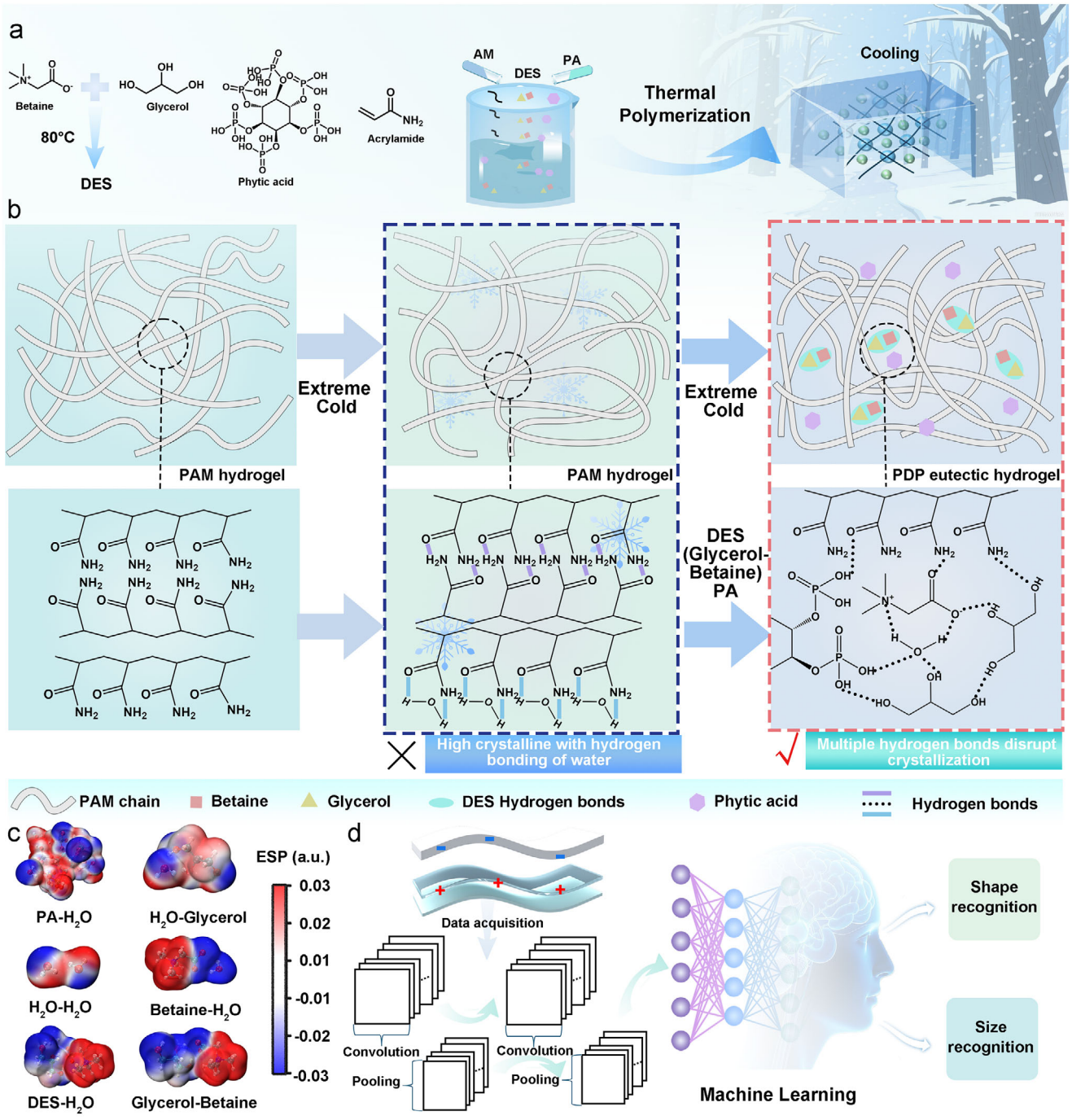

Figure 1. a) Preparation of PDP eutectic hydrogel. b) Schematic illustration of PDP eutectic hydrogel using PA and DES strategy for functioning in extreme cold. c) The distribution of molecular electrostatic potential surfaces. d) Applications of PDP eutectic hydrogel.

that the storage modulus (G′) consistently exceeded the loss modulus (G″) across both strain and frequency sweeps, indicating predominantly elastic behavior (Figure 2d; Figure S4, Supporting Information). The loading-unloading tensile curves (Figure 2e,f) demonstrate a decrease in hysteresis and an increase in resilience with increasing strain. At low tensile strains, dynamic crosslinking hydrogen bonds within the PDP eutectic hydrogel break to dissipate energy, leading to significant hysteresis loss. As strain increases, the dynamic crosslinking network undergoes rapid reorganization to achieve uniform stress distribution, which reduces local energy concentration and thereby minimizing losses in subsequent cycles. In the continuous loading and unloading process from 10–100% strain and the loading-unloading curves at different rates of 100% strain (Figures S5 and S6a, Supporting Information), the stress–strain curves almost overlap, indicating excellent cyclic stability. Even after 400 cycles at 40% strain,

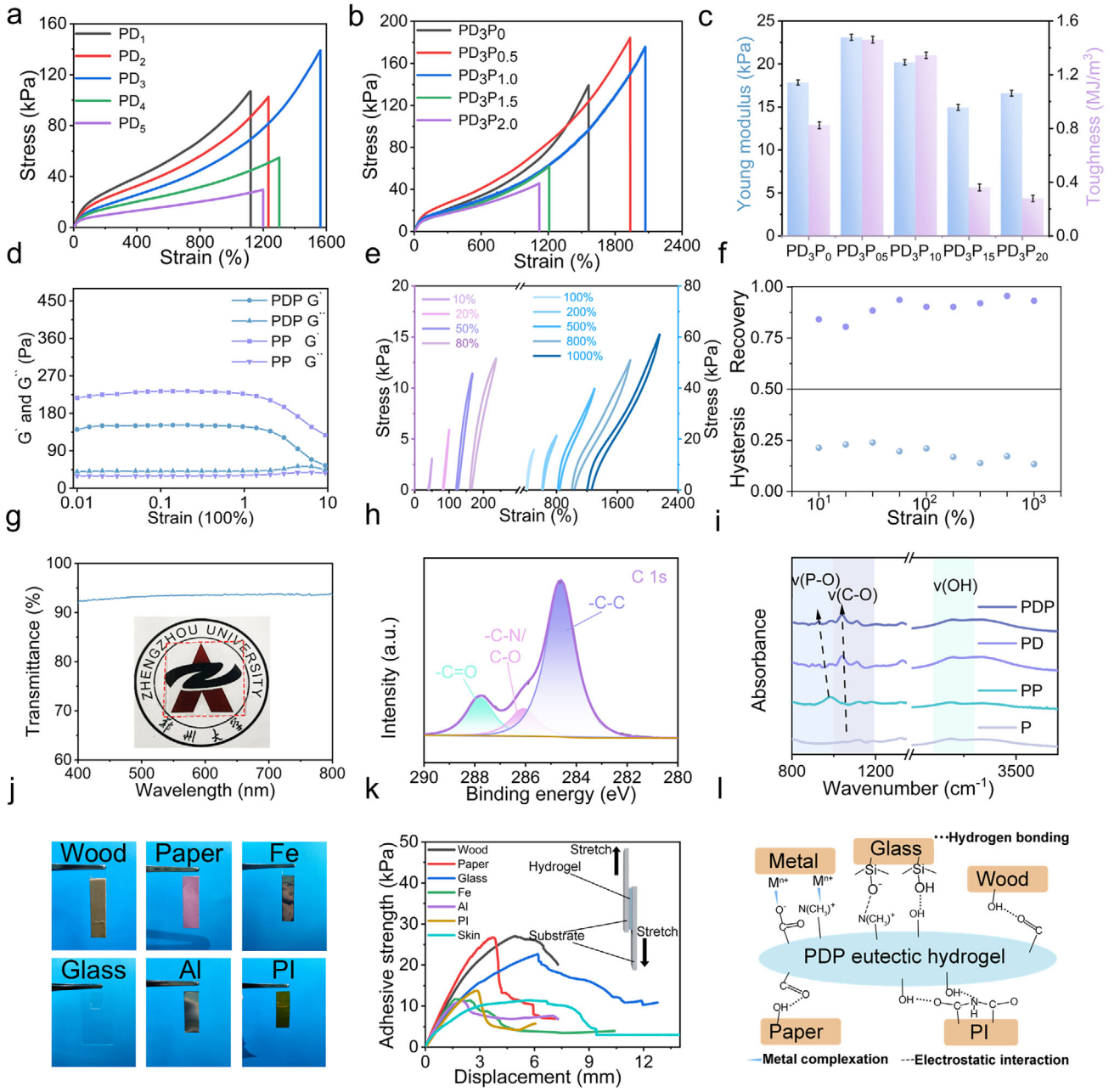

Figure 2. Characterization and mechanical properties. a,b) Stress–strain curves of PDP eutectic hydrogel with varying DES contents (a) and PA contents (b). c) Toughness and elastic modulus of PDP eutectic hydrogel with different PA contents. d) The strain-dependent changes of G'' and G' of PDP eutectic hydrogel and PP hydrogel. e) Loading-unloading tensile curves of PDP eutectic hydrogel within a strain range of 10% to 1000%. f) Elasticity and hysteresis of PDP eutectic hydrogel within a strain range of 10–1000%. g) UV–vis transmittance of PDP eutectic hydrogel, and a photograph of PDP eutectic hydrogel. h) The high-resolution XPS spectra for C respectively. i) FTIR spectra of PAM hydrogel, PP hydrogel, PD hydrogel, and PDP eutectic hydrogel. j) Visual demonstration of the adhesion of PDP eutectic hydrogel to various. k) Adhesion mechanical curves. l) Possible interactions between the PDP eutectic hydrogel and various substrates.

the hydrogel maintains stable mechanical properties, demonstrating robust resistance to fatigue (Figure S6b, Supporting Information).

The PDP eutectic hydrogel exhibits high optical transparency, as visually demonstrated by a digital photograph showing the hydrogel placed atop the Zhengzhou University emblem without obscuration obscuring it. UV–vis spectroscopy further confirms that its transmittance exceeds 90% across the entire visible spectrum (400–800 nm) (Figure 2g). The chemical structure of PDP eutectic hydrogel is characterized by Fourier transform infrared spectroscopy (FTIR), Raman spectroscopy (RS), and X-ray photoelectron spectroscopy (XPS) (Figures S7–S9, Supporting

Information). XPS analysis reveals the presence of C, N, and O elements. Analysis of the FTIR spectrum shows a broad stretching vibration of —N—H bonds at 3330 cm^{-1} and a stretching vibration of —C—N bonds at 1110 cm^{-1}. The N 1s peak in XPS is located at 399.4 eV corroborates the FTIR findings (Figure S9b, Supporting Information). A stretching vibration of —C═O bonds appear at 1658 cm^{-1}, and a stretching vibration of —C—O bonds is observed at 1040 cm^{-1}. The O 1s peak at 531.5 eV and C 1s peak at 285 eV in XPS further validated the infrared analysis (Figure 2h; Figure S10c, Supporting Information). Meanwhile, RS also proves the existence of the aforementioned covalent bonds (Figure S8, Supporting Information). FTIR analysis of Figure 2i shows that both the PDP eutectic hydrogel and the (PAM/DES) PD eutectic hydrogel exhibit infrared absorption peaks of —C—O bonds at 1040 cm^{-1}. The (PAM/PA) PP hydrogel and PDP eutectic hydrogel both display characteristic absorption peaks at 980 and 928 cm^{-1}, which are attributed to the vibrational characteristics of —P—OH groups. When DES is introduced into the system, the absorption peak of the —P—OH group undergoes a significant redshift, due to the formation of hydrogen bonding interactions between DES and —P—OH groups that lower their vibrational frequency.

The adhesion plays a critical role in the sensing performances of flexible sensors, and the PDP eutectic hydrogel exhibits strong and versatile adhesive capabilities. As shown in Figure 2j, the PDP eutectic hydrogel exhibits strong interfacial adhesion to diverse substrates, including metals, wood, paper, skin, and polyimide (PI). The adhesion performance was further quantified via lap-shear measurements (Figure 2k). The hydrogel achieves maximum adhesive strengths of 27.03 kPa on wood, 11.40 kPa on skin, 11.43 kPa on iron, 26.7 kPa on paper, 13.7 kPa on PI, 11.21 kPa on aluminum, and 22.65 kPa on glass (Figure S10, Supporting Information), demonstrating its robust and substrate-independent adhesion. The PDP eutectic hydrogel contains multiple functional groups, which are crucial for its adhesive behavior, as verified by its chemical structure analysis (Figure 2l).

2.3. Antifreezing Properties of the PDP Eutectic Hydrogel

The PDP eutectic hydrogel exhibits remarkable antifreezing performance, which can be primarily attributed to the strong intermolecular interactions within the DES phase that inhibit the crystallization of free water.[39–41] These effects are closely related to the hydrogen bonding interactions between the DES components and water. To further analyze and understand the hydrogen bonding interactions in PDP eutectic hydrogel, temperature-dependent FTIR spectroscopy (30–150 °C) and generalized 2D correlation spectroscopy (2DCOS) are investigated (**Figure 3**a). As the temperature increases, the intensities of the -NH_2 and —OH peak decrease significantly (Figure 3b). Notably, the —OH peak undergoes a blueshift to higher wavenumbers, indicating the transition of hydroxyl groups from hydrogen-bonded to free states. Simultaneously, the peak intensity of hydrogen-bonded —C═O groups (centered at ≈1667 cm^{-1}) also decreases significantly (Figure 3c). These spectral changes confirm that elevated temperatures disrupt hydrogen bonds between —OH···OH and —OH···NH_2 groups, supporting the existence of dynamic hydrogen bonding networks within the hydrogel. These findings clearly demonstrate the formation of hydrogen bonds in the PDP eutectic hydrogel, providing key mechanistic insights into its hydrogen bonding behavior.[42] To further analyze the synergistic effect between solvent molecules in PDP eutectic hydrogel, the binding energies between DES and water are calculated by density functional theory (DFT) (Figure 3d). The DFT analysis shows that glycerol and betaine exhibit the highest binding energies, highlighting the intrinsic stability of the DES complex. In contrast, the binding energy of H_2O–H_2O (8.5 kcal mol^{-1}) is lower than those between water and DES components, indicating that DES-H_2O hydrogen bonding is thermodynamically more favorable. These findings suggest that the DES-H_2O binary solvent system and electronegative polar groups synergistically weaken the strong hydrogen bonding interactions between water molecules in the PDP eutectic hydrogel (Figure 3e).

Differential scanning calorimetry (DSC) is performed to study the effect of DES on the freezing behavior of hydrogels (Figure 3f). The peak at −13.7 °C corresponds to the PP hydrogel. Notably, the PDP eutectic hydrogel shows a significantly reduced freezing point of −34.3 °C upon DES incorporation, indicating enhanced cryotolerance. These results are consistent with the rheological analysis in Figure 3g, where the modulus of the PP hydrogel increases rapidly at ≈−10 °C due to ice crystallization, while the modulus of PDP eutectic hydrogel containing DES remains stable, further confirming its antifreezing capability. Mechanical flexibility at low temperatures is also evaluated in detail. The PDP eutectic hydrogel maintains stretchability, twistability, and foldability at both 20 and −20 °C, confirming its mechanical robustness under cryogenic conditions (Figure 3h). As described in Figure S11 (Supporting Information), the PDP eutectic hydrogel maintains good electrical conductivity at low temperatures, as demonstrated by its ability to light up an LED at −20 °C. The water retention performance is assessed by monitoring the mass change under ambient conditions in a windless environment (Figure S12, Supporting Information). After 72 h, the PP hydrogel loses 68.9% of its mass, whereas the PDP eutectic hydrogel shows a relatively low mass change. This is attributed to the intermolecular forces between DES and water molecules, which prevent excessive water evaporation. Figure S13 (Supporting Information) shows that the PDP eutectic hydrogel remains flexible after 12 h of ambient storage, indicating good durability and expanding its potential for practical applications in diverse environments.

2.4. Sensing Properties of PDP Eutectic Hydrogel

During tensile deformation, the cross-sectional area of the PDP eutectic hydrogel is progressively reduced by the Poisson effect, triggering structural compression of ion transport channels through strain energy transfer. This collapse of conductive pathways reduces ionic mobility, thereby increasing electrical resistance as demonstrated in **Figure 4**a. Notably, the introduction of PA into the PDP eutectic hydrogel yields a substantial enhancement in ionic conductivity, reaching 87.35 mS m^{-1} with a remarkable 820% increase (Figure 4b). This improvement arises from the dissociation of phosphate groups in PA, which releases hydrogen ions and facilitates ion transport. Figure 4c defines the slope of the $\Delta R/R_0$ curve as GF, which is used to evaluate the sensitivity of the strain sensor based on the PDP eutectic hydrogel. To

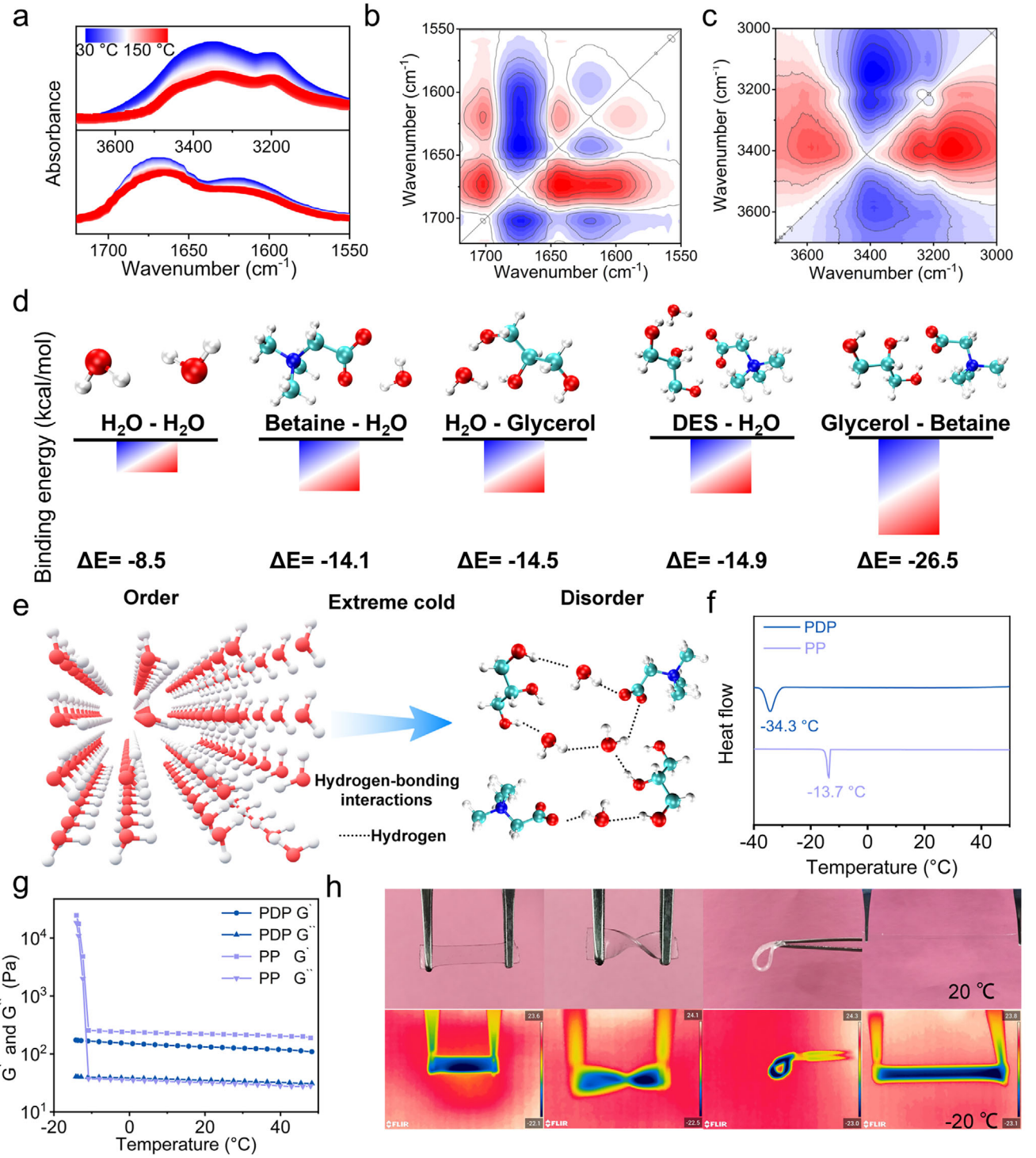

Figure 3. Antifreezing properties of the PDP eutectic hydrogel. a) Temperature-dependent FTIR spectra of PDP eutectic hydrogel. b,c) The corresponding 2DCOS map in the wavenumber range of 1550–1750 cm^{-1} (b) and 3000–3700 cm^{-1} (c). d) The binding energy between H_2O, glycerol, betaine and DES. e) Schematic illustration of antifreezing mechanism in eutectic hydrogel. f) DSC curves of PP hydrogel and PDP eutectic hydrogel. g) The rheological temperature scanning spectra of PDP eutectic hydrogel and PP hydrogel at a constant frequency of 10 rad s^{-1} and 1 % strain show their G′ and G″. h) The stretching, twisting and folding of the PDP eutectic hydrogel at 20 and −20 °C.

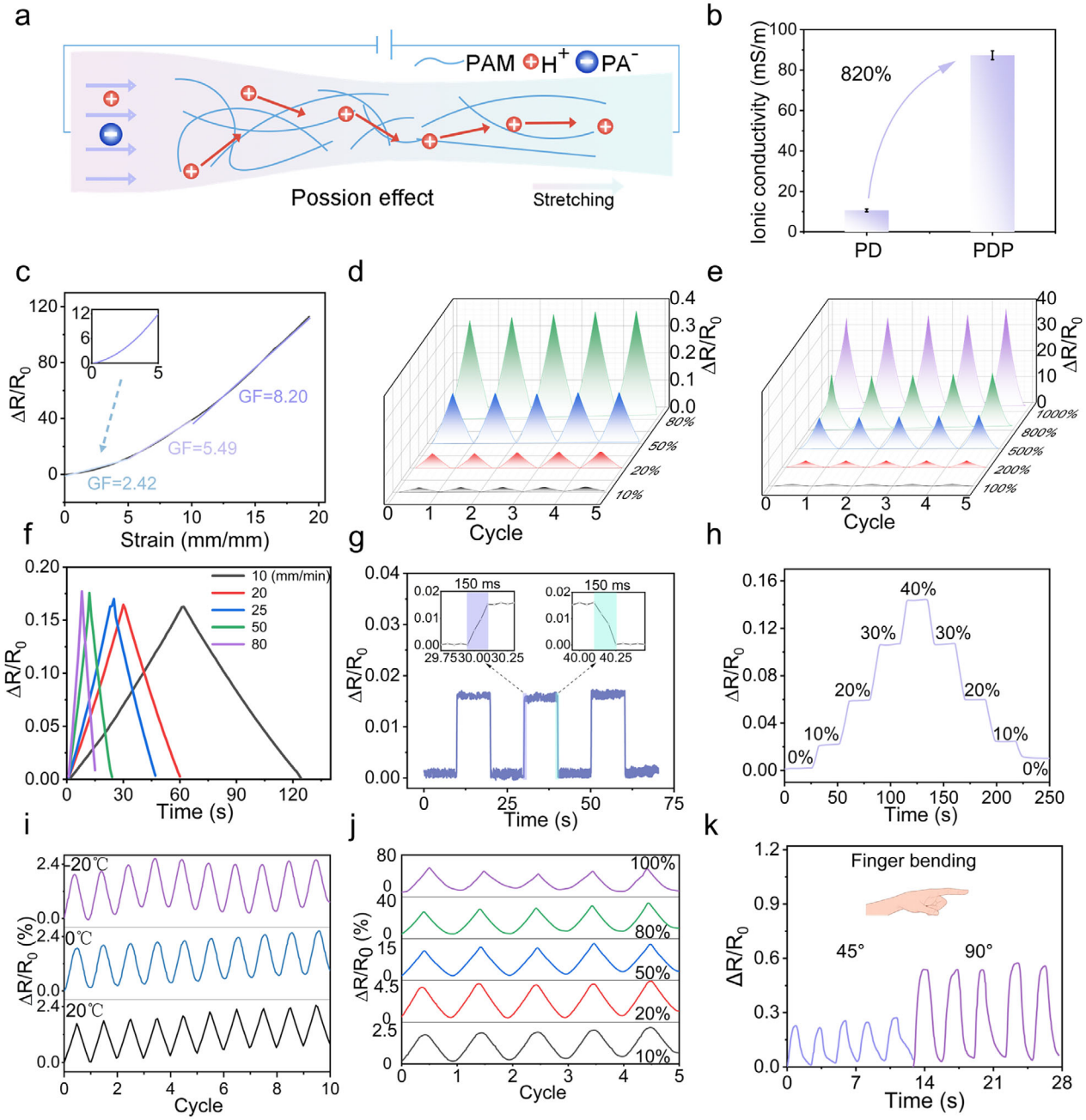

Figure 4. Strain sensing properties of the PDP eutectic hydrogel. a) The conduction mechanism of the PDP eutectic hydrogel. b) Comparison of the electrical conductivity between PD eutectic hydrogel and PDP eutectic hydrogel. c) Resistance-strain curves of the PDP eutectic hydrogel-based strain sensors. d,e) $\Delta R/R_0$ at various small strains (d) and large strains (e). f) Relative resistance changes at different stretching-releasing rates at 40% strain. g) The response time of the PDP eutectic hydrogel strain sensor. h) The voltage-rising and recovery response curves of PDP eutectic hydrogel within different strain ranges. i) The resistance changing curves of the PDP eutectic hydrogel after ten cycles of tensile recovery at 10% strains at different temperatures. j) The resistance changing curves of the PDP eutectic hydrogel after five cycles of tensile recovery at 10–100% strains. k) Variation of relative resistance at different degrees of finger bending.

ensure accurate measurement of resistance changes in the PDP eutectic hydrogel during mechanical straining, silver paste is employed to minimize contact resistance (Figure S14, Supporting Information). Through meticulous mathematical fitting, three distinct GF values are identified across different strain regimes: 2.42 (0–500% strain), 5.49 (500–1000% strain), and 8.20 (>1000% strain). The variation in GF across different strain regimes arises from the coupled response of the PDP eutectic hydrogel's network architecture and the dynamic evolution of its ion-conductive pathways, which is intrinsically governed by the compositional

roles of PA, DES, and PAM. These findings clearly demonstrate the high sensitivity of the sensor across a broad strain spectrum. As shown in Figure 4d, the PDP eutectic hydrogel exhibits excellent repeatability and high sensitivity within the strain range of 10–80%, which is crucial for monitoring small human motions. The stable signal output in the strain range of 100–1000% further confirms its good sensing stability (Figure 4e). As shown in Figure 4f, the sensing performance remains consistent under different stretching speeds at 40% strain, demonstrating speed-independent response behavior. Additionally, both the response time and recovery time are 150 ms, further confirming its rapid responsiveness, which is critical for real-time monitoring of sensing signals (Figure 4g). The PDP eutectic hydrogel also displays stable stepwise signals under intermittent strain inputs, further validating its dynamic reliability (Figure 4h). Furthermore, the PDP eutectic hydrogel can still output stable electrical signals after completing 200 loading-unloading cycles at 40% strain (Figure S15, Supporting Information). The stable response of electrical signals meets the requirements of most application scenarios, underscoring its excellent durability and long-term operational stability for practical sensing applications.

As depicted in Figure 4i, the PDP eutectic hydrogel maintains stable electrical signals during continuous loading-unloading at 10% strain under various temperature conditions of 20, 0, and −20 °C. Notably, even under a wide strain range of 10–100% at −20 °C, the hydrogel consistently exhibits repeatable and robust sensing performance, highlighting its excellent low-temperature operational stability (Figure 4j). As shown in Figure 4k, the $\Delta R/R_0$ values increase correspondingly with finger bending angles of 45° and 90° and remain stable at each fixed angle. Similar stable $\Delta R/R_0$ signals are observed during wrist motion and knee bending, confirming the consistent performance of the PDP eutectic hydrogel (Figure S16a,b, Supporting Information). Additionally, the PDP eutectic hydrogels demonstrated excellent sensing stability in detecting subtle strains, such as facial expressions like frowning (Figure S16c, Supporting Information), and cheek puffing (Figure S16d, Supporting Information). These results collectively demonstrate the hydrogel's excellent capability for both macroscopic and micro-motion detection, establishing it as a promising candidate for multifunctional wearable sensing systems. The prepared PDP eutectic hydrogel possesses excellent mechanical properties and is well suited for wearable flexible strain sensors with high stretchability and high GF requirements (Figure S17, Supporting Information).

2.5. Electrical Output Performance of PDP-TENG

The PDP eutectic hydrogel displays outstanding flexibility and elasticity, sustaining structural integrity under diverse complex deformations, including stretching, twisting, bending, and folding. These mechanical properties enable the hydrogel-based PDP-TENG to adapt seamlessly to diverse working conditions and application scenarios, such as conformal integration with human skin in wearable electronics or efficient energy harvesting from irregular surfaces. The PDP-TENG is constructed as a sandwich-structured device operating in single-electrode mode, which enhances its practicality for real-world applications. It consists of a PU film as the positive triboelectric layer and a PDP eutectic hydrogel as the electrode. When Ecoflex, employed as the dielectric material, comes into contact with the PU layer, triboelectric charges of equal magnitude and opposite polarity are generated at the interface, with Ecoflex gaining negative charges (**Figure 5a-i**). As Ecoflex separates from the PDP-TENG, the resulting electrostatic imbalance drives a flow of electrons within the external circuit, inducing negative charges on the hydrogel electrode (Figure 5a-ii). This current ceases once Ecoflex is fully detached (Figure 5a-iii). When Ecoflex approaches the PDP-TENG again, the electrostatic induction reverses, causing electrons to flow back into the hydrogel layer (Figure 5a-iv). Additionally, finite-element simulations using COMSOL Multiphysics illustrate the potential distribution under various operating states, providing visual insight into the device's working mechanism (Figure 5b).

To characterize the performance of PDP-TENG under practical mechanical stimuli with varying magnitudes and frequencies, the effects of pressure and frequency on its open-circuit voltage (V_{OC}), short-circuit current (I_{SC}), and short-circuit transferred charge (Q_{SC}) are systematically evaluated. As shown in Figure 5c–e, under a constant testing frequency of 2 Hz and a triboelectric contact area of 20 mm × 20 mm, increasing the applied pressure from 0.1 to 15 N leads to a notable enhancement in output signals: V_{OC} increases from 20 to 60 V, I_{SC} from 0.06 to 0.66 μA, and Q_{SC} from 5 to 20 nC. This enhancement is attributed to the enlarged effective contact area at higher pressures, which facilitates the generation of more triboelectric charges. Figure 5f illustrates the voltage-based sensitivity of PDP-TENG under varying pressures, yielding sensitivities of 6.71 V kPa^{-1} in the low-pressure regime and 0.29 V kPa^{-1} in the high-pressure regime. The frequency-dependent performance is further explored at a fixed pressure of 10 N (Figure 5g; Figure S18b, Supporting Information). V_{OC} and Q_{SC} remain nearly constant across frequencies from 1 to 5 Hz, indicating the robust signal stability of the PDP eutectic hydrogel electrode. In contrast, I_{SC} increases with frequency, due to a higher charge transfer rate at elevated working frequencies (Figure S18a, Supporting Information). As depicted in Figure 5h, the response and recovery times are determined to be 86 and 62 ms, respectively, which are sufficient to meet the requirements of real-time dynamic sensing. Furthermore, the PDP-TENG exhibits outstanding durability, as evidenced by the negligible voltage degradation after 4000 continuous cycles at 10 N and 2 Hz (Figure 5i).

As shown in Figure 5j, a rectifier is used to supply power to external electronic devices. In Figure 5k and Figure S19 (Supporting Information), under a 10 N load at 1 Hz, the charging time of the capacitor increases with capacitance. As shown in Figure 5l, the voltage during the contact-separation cycle is 20 mV when charging the capacitor, indicating a stable increase in the continuous charging process. At a constant load of 10 N, increasing the operating frequency significantly improves the charging rate for a 1 μF capacitor. To systematically evaluate the energy-harvesting performance of the PDP-TENG under different external load conditions, Figure S20 (Supporting Information) presents its output characteristics—including V_{OC}, I_{SC}, and instantaneous power density—across load resistances ranging from 1 kΩ to 10 GΩ. The power-density analysis reveals a maximum output of 45 mW m^{-2} at an optimal matching resistance of 100 MΩ, highlighting the device's efficient charge-transfer

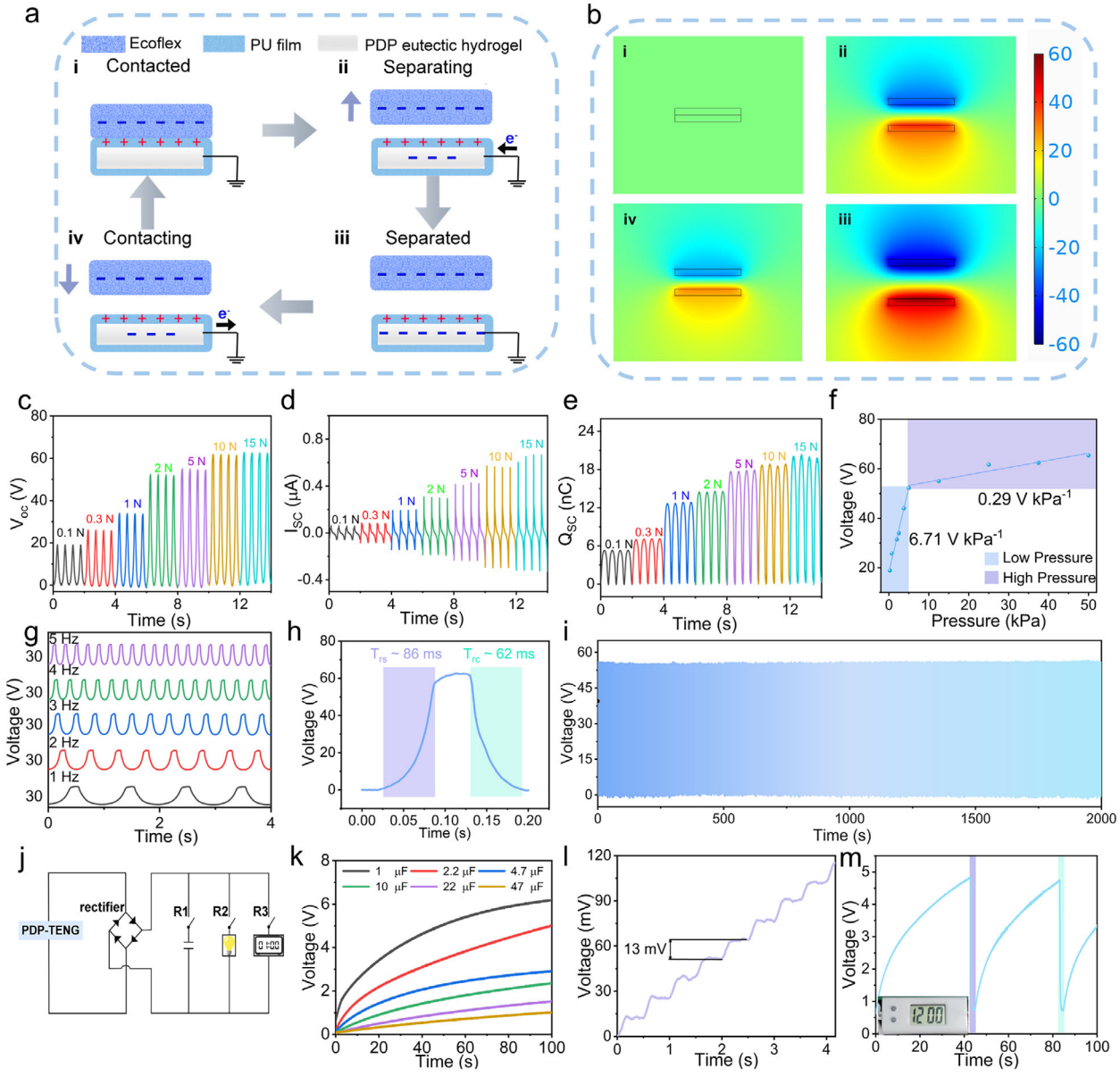

Figure 5. Working mechanism and output performance characterization of the PDP-TENG. a) Schematic diagram of the PDP-TENG structure. b) COMSOL simulation of the corresponding potential distribution of PDP-TENG. c–e) V_{OC} (c), I_{SC} (d) and Q_{SC} (e) the PDP-TENG under varying applied pressures. f) Sensitivity analysis of PDP-TENG in the pressure range of 0–50 kPa. g) V_{OC} of PDP-TENG at different frequencies under a pressure of 10 N. h) The response time of PDP-TENG. i) Stability of the V_{OC} during 4000 contact-separation cycles at 2 Hz and 10 N. j) Schematic circuit diagram of PDP-TENG connected to capacitor and load. k) Charging curves of the PDP-TENG for capacitors with different capacitances at a frequency of 1 Hz. l) The voltage increments per cycle. m) The PDP-TENG powering an electronic watch through a connected circuit.

capability over a broad dynamic load window and underscoring its promise for practical energy-harvesting applications (Figure S21, Supporting Information).

Furthermore, owing to the high-power density and remarkable output performance of the PDP-TENG, it can stably supply power to electronic devices. As depicted in Figure 5m, the energy generated by the PDP-TENG stored in a 1 μF capacitor, which is charged at a frequency of 2 Hz for 40 s, is sufficient to power an electronic watch. In addition, the harvested energy can easily light up 20 LEDs (Figure S22, Supporting Information). These results highlight the efficacy of the self-powered device in driving electronic timing equipment and its great potential in future energy-harvesting applications.

2.6. Application of PDP Eutectic Hydrogel

Soft robotic grippers are among the most widely used soft machines, relying on deformation to grasp and manipulate objects. The PDP-TENG, with its high flexibility and sensitive

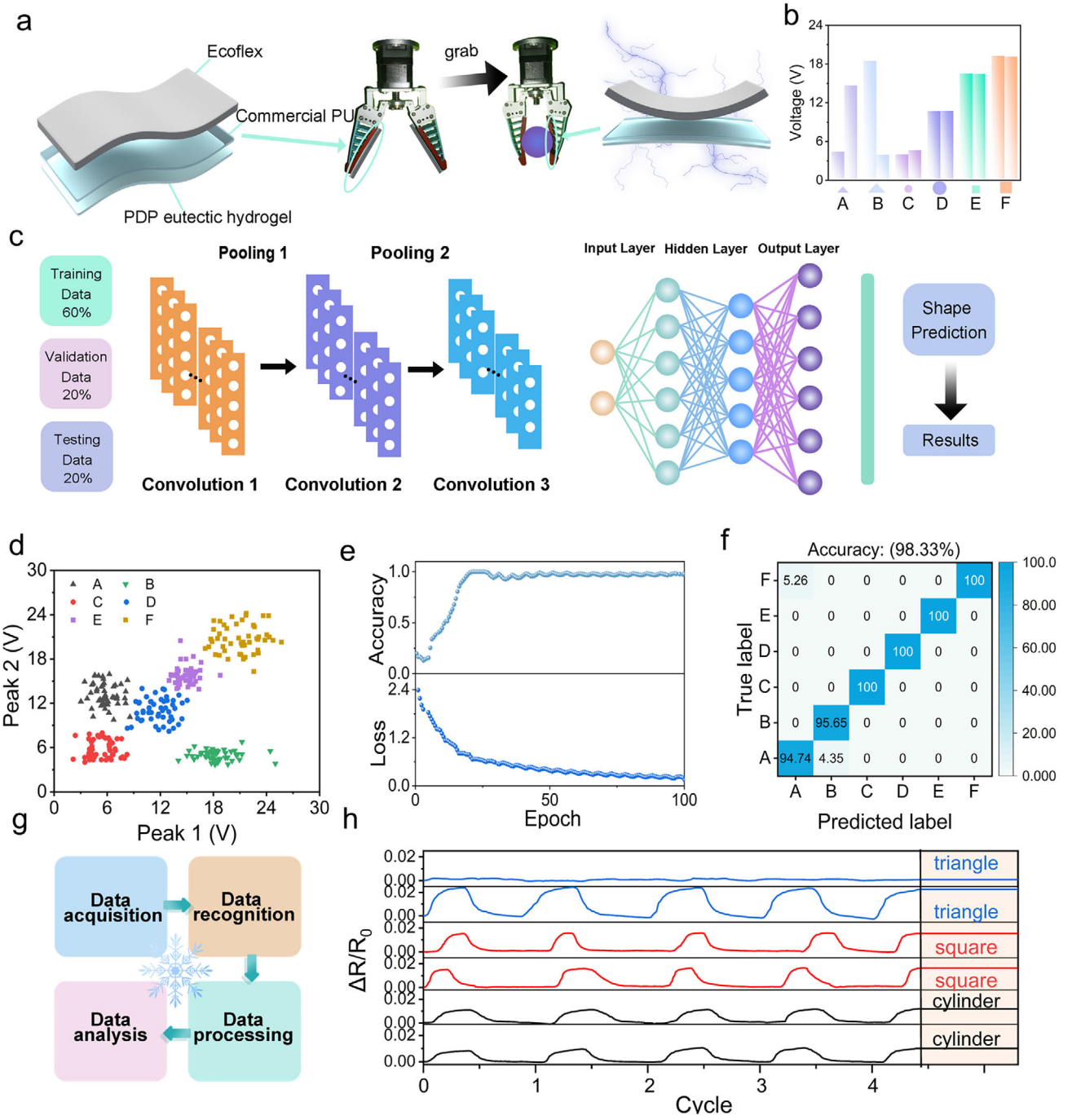

Figure 6. Machine learning-assisted object recognition by the soft robotic gripper system. a) Schematic illustration of the robotic gripper integrated with PETS and tactile sensors. b) Voltage signal of the sensors during grasping of objects with different geometries. c) Schematic of the CNN model used for object recognition. d) Data visualization of voltage signals collected from grasping six different-shaped objects. e) Evaluation of the model's accuracy and loss function over 100 training epochs. f) Confusion matrix for recognition and grasping. g) Schematic diagram of the process of the soft robotic gripper at low temperatures. h) Resistive signal curves of the gripper during object grasping.

electrical response, plays a critical role in enhancing the sensing capabilities of such systems. A PDP/Ecoflex-TENG sensor (PETS), composed of the PDP-TENG and Ecoflex dielectric layer, is integrated into a soft robotic gripper to enable object shape recognition during grasping (**Figure 6a**). Each gripper finger is equipped with a PETS connected to a voltage signal acquisition device. To validate its performance, grasping tests are conducted using six objects of different shapes: isosceles triangles with heights of 2 and 4 cm, cylinders with diameters of 2 and 4 cm, and squares with side lengths of 2 and 4 cm. During

repeated grasping tests, the PETS sensors on the gripper fingers generated distinct voltage signal profiles corresponding to each object (Figure 6b). The unique voltage amplitudes and polarities generated during contact-separation motions enabled reliable inference of object type based on triboelectric signals. For each object, 50 sets of triboelectric voltage data collected by the two PETS are subjected to feature extraction (Figure 6d; Figures S23 and S24, Supporting Information). This study adopts a 1D convolutional neural network (1D-CNN) model for target recognition tasks. The network can effectively capture the temporal and spatial features in data through its local receptive field and weight sharing mechanisms. The dataset is randomly split into training (60%), testing (20%), and validation (20%) sets. After post-processing, the signals are fed into a CNN model for classification (Figure 6c). The model demonstrates high classification accuracy and stability after 100 training epochs. Performance evaluation of the proposed machine learning algorithm was conducted using training accuracy and loss function curves, which shows that the model achieved excellent classification accuracy and stability following rigorous training over 100 epochs (Figure 6e). A confusion matrix analysis further confirmed the model's robust performance, achieving an overall classification accuracy of 98.33% (Figure 6f). These results highlight the potential of PETS-enabled grippers for intelligent shape recognition during soft robotic manipulation. Integration with more complex systems, such as multi-fingered robotic hands, could further expand the range of detectable object geometries.

The PDP eutectic hydrogel also exhibits exceptional antifreeze properties, enabling its integration with soft robotic grippers to grasp objects and perform shape recognition at low temperatures (Figure 6g). During repeated cold-temperature grasping of different objects, the two sensor-integrated grippers exhibit stable, distinct resistive signal changes, which are attributed to variations in contact area between the object's shape and gripper surface (Figure 6h). This demonstration highlights the potential of PDP eutectic hydrogel-based sensors for reliable tactile sensing in freezing environments, underscoring their applicability in soft robotics operating under extreme conditions.

3. Conclusion

In conclusion, we have developed PDP eutectic hydrogels by partially replacing water with DES and introducing PA as a conductive filler. The rich variety of functional groups in DES facilitates strong molecular interactions with the hydrogel network, thereby imparting outstanding water retention and antifreeze properties. Meanwhile, the abundant ionizable protons in PA endow the PDP eutectic hydrogel with excellent ionic conductivity. These features enable the flexible electrodes based on PDP eutectic hydrogels to exhibit enhanced sensing performance when integrated with deep learning algorithms, allowing for complex tasks such as shape recognition. Collectively, the synergistic integration of environmental durability, mechanical adaptability, ionic conductivity, and data-driven functionality underscores the promise of PDP eutectic hydrogels in next-generation flexible electronics and intelligent sensing systems.

4. Experimental Section

Materials: The following reagents used in this study were purchased from the indicated companies: Acrylamide (AM, 99%) and ammonium persulfate (APS) were obtained from Aladdin Chemistry Co., Ltd. N, N'-methylene-bis-acrylamide (MBAA, 99%), betaine and phytic acid were acquired from Macklin Biochemical Co. Glycerol was purchased from Chengdu Kelong Chemical Co., Ltd. Ecoflex rubber (00–30) was supplied by Smooth-On Co. Ltd., America.

Synthesis of PDP Eutectic Hydrogel: Glycerol and betaine were mixed at 80 °C for 2 h to form DES. AM (3 g) and PA (0.5 g) were copolymerized by free radical copolymerization in the presence of DES (3 g) and H_2O (7 g). MBA (2 mg) was used as crosslinking agent and APS (10 mg) was used as initiator. Subsequently, the uniform mixture was poured into the mold, and finally polymerized at 65 °C for 3 h to prepare PDP eutectic hydrogel.

Characterization: XPS analysis was performed using a Thermo Fisher-K-Alpha spectrometer to investigate the elemental composition and chemical states. FTIR spectra were recorded using a Thermo Scientific Nicolet iS50 spectrometer, while Raman spectra were acquired with a HORIBA-LabRAM HR Evolution. DSC measurements were performed using a NETZSCH-DSC 200 F3. Rheological behavior was examined using a HAAKE MARS IQ Air. Infrared photographs were recorded using a FLIR E86 24° infrared thermal imager. Measurements of the output voltage and force of the PDP-TENG were carried out using an electrometer (Keithley 6514) and a linear motor (LinMot E1100) coupled with a commercial force sensor (501F01, YMC Piezotronics INC).

Supporting Information

Supporting Information is available from the Wiley Online Library or from the author.

Acknowledgements

The authors acknowledge the financial support of this research by the National Natural Science Foundation of China (52303114, 52173048, 52573100, 52125205, 52532005, and 52250398), China Postdoctoral Science Foundation (2023M733199, 2024T170838), Henan Province University Scientific and Technological Innovation Talent Support Program (26HASTIT047), Henan Provincial Outstanding Youth Science Fund Rolling Project (252300421238), National Key Research and Development (R&D) Program from Ministry of Science and Technology of China (2024YFB3814100), and the Fundamental Research Funds for the Central Universities. The authors also thank Xuzhou B&C Chemical Co. Ltd for providing the photoresist (HTA116, HTA112, B&C Chemicals) used in the work.

Conflict of Interest

The authors declare no conflict of interest.

Data Availability Statement

The data that support the findings of this study are available from the corresponding author upon reasonable request.

Keywords

antifreezing, deep eutectic solvent, eutectic hydrogel, machine learning, triboelectric nanogenerator

Received: October 30, 2025
Revised: November 26, 2025
Published online:

[1] Y. Chen, C. Lv, X. Ye, J. Ping, Y. Ying, L. Lan, *Matter.* **2025**, *8*, 101992.
[2] W. Yang, S. Liu, Z. Wang, H. Liu, C. Pan, C. Liu, C. Shen, *Nano. Energy.* **2024**, *127*, 109799.
[3] H. Li, T. Lv, H. Sun, G. Qian, N. Li, Y. Yao, T. Chen, *Nat. Commun.* **2019**, *10*, 536.
[4] Y. Zhao, X. Zhang, Y. Hao, Y. Zhao, P. Ding, W. Zhai, K. Dai, G. Zheng, C. Liu, C. Shen, *Adv. Compos. Hybrid. Mater.* **2024**, *7*, 245.
[5] X. Huang, C. Chen, X. Ma, T. Zhu, W. Ma, Q. Jin, R. Du, Y. Cai, M. Zhang, D. Kong, M. Wang, J. a. Ren, Q. Zhang, X. Jia, *Adv. Funct. Mater.* **2023**, *33*, 2302846.
[6] F. Li, D. Lyu, S. Liu, W. Guo, *Adv. Mater.* **2020**, *32*, 1806538.
[7] M. Bai, Y. Chen, L. Zhu, Y. Li, T. Ma, Y. Li, M. Qin, W. Wang, Y. Cao, B. Xue, *Nat. Commun.* **2024**, *15*, 10569.
[8] Y. Wei, L. Xiang, H. Ou, F. Li, Y. Zhang, Y. Qian, L. Hao, J. Diao, M. Zhang, P. Zhu, Y. Liu, Y. Kuang, G. Chen, *Adv. Funct. Mater.* **2020**, *30*, 2005135.
[9] G. Wu, X. Li, R. Bao, C. Pan, *Adv. Funct. Mater.* **2024**, *34*, 2405722.
[10] X.-F. Zhang, X. Ma, T. Hou, K. Guo, J. Yin, Z. Wang, L. Shu, M. He, J. Yao, *Angew. Chem., Int. Ed.* **2019**, *58*, 7366.
[11] H. Sun, Y. Zhao, S. Jiao, C. Wang, Y. Jia, K. Dai, G. Zheng, C. Liu, P. Wan, C. Shen, *Adv. Funct. Mater.* **2021**, *31*, 2101696.
[12] J. He, R. Wei, X. Ma, W. Wu, X. Pan, J. Sun, J. Tang, Z. Xu, C. Wang, C. Pan, *Adv. Mater.* **2024**, *36*, 2401931.
[13] S. Sun, S. Hao, Y. Liu, S. Sun, Y. Xu, M. Jiang, C. Shao, J. Wen, R. Sun, *ACS Nano* **2025**, *19*, 811.
[14] X. Dong, X. Guo, Q. Liu, H. Qi, G. Zou, T. Li, H. Gao, W. Zhai, *Mater. Today* **2024**, *72*, 25.
[15] Y. Shao, C. Dang, H. Qi, Z. Liu, H. Pei, T. Lu, W. Zhai, *Matter.* **2024**, *7*, 4076.
[16] B. Wang, A. Lv, H. Wu, B. Guo, Y. Lu, Z. Chang, Y. Wu, X. Li, Q. Yang, J. Nie, J. Wei, Q. Ren, D. Ji, Y. Zhang, M. Y. Rotenberg, Y. Fang, *ACS Nano* **2025**, *19*, 8176.
[17] K. Xue, C. Shao, J. Yu, H. Zhang, B. Wang, W. Ren, Y. Cheng, Z. Jin, F. Zhang, Z. Wang, R. Sun, *Adv. Funct. Mater.* **2023**, *33*, 2305879.
[18] S. Zhang, C. Li, *Adv. Funct. Mater.* **2025**, *35*, 2416599.
[19] J. Lee, S. Kim, J. W. Kim, J. Kim, Y. Choi, M. Park, D. S. Kim, H. Lee, S. Kim, Y. Kim, J. S. Ha, *Small* **2025**, *21*, 2409365.
[20] Z. Cheng, M. Kang, X. Peng, L. Ren, J. Xie, Q. Yuan, X. Xu, J. Li, *Adv. Mater.* **2025**, *37*, 2412866.
[21] B. Guo, M. Yao, S. Chen, Q. Yu, L. Liang, C. Yu, M. Liu, H. Hao, H. Zhang, F. Yao, J. Li, *Adv. Funct. Mater.* **2024**, *34*, 2315656.
[22] H. Xu, H. Li, Y. Zhang, Y. Guan, Y. Zhang, *Nano-Micro Lett.* **2024**, *11*, 2400938.
[23] C. Zhou, X. Song, R. Wei, S. Liu, Z. Wu, H. Chen, *Chem. Eng. J.* **2024**, *499*, 155992.
[24] W. Liu, C. Jiang, X. Li, H. Li, Y. Zhang, Y. Huang, S. Chen, Q. Hou, *Carbohydr. Polym.* **2024**, *328*, 121741.
[25] X. Jiang, Y. Hou, Y. Wang, F. Chu, J. Zhu, L. Song, Y. Hu, W. Hu, *Adv. Funct. Mater.* **2025**, *35*, 2412313.
[26] Y. Zhang, Y. Wang, Y. Guan, Y. Zhang, *Nat. Commun.* **2022**, *13*, 6671.
[27] H. Wu, J. Song, N. Gao, X. Pang, Y. Li, Z. Xu, X. Yu, *Chem. Eng. J.* **2025**, *505*, 159714.
[28] J. D. Mota-Morales, E. Morales-Narváez, *Matter* **2021**, *4*, 2141.
[29] L. Song, Z. Wang, S. Chen, Y. Shen, J. Yin, R. Wang, *Adv. Mater.* **2025**, *37*, 2417978.
[30] Y. Liu, J. Tao, Y. Mo, R. Bao, C. Pan, *Adv. Mater.* **2024**, *36*, 2313857.
[31] Z. Su, H. Guo, C. Zhao, *Nano-Micro Lett.* **2023**, *15*, 96.
[32] Y. Cheng, C. Yang, T. Zhu, C. Wu, J. Huang, Y. Lai, *Adv. Funct. Mater.* **2025**, *35*, 2415533.
[33] M. Pan, G. Zhao, C. Ding, B. Wu, Z. Lian, H. Lian, *Carbohydr. Polym.* **2017**, *176*, 307.
[34] Q. Zeng, X. Lai, H. Li, Z. Chen, X. Zeng, L. Zhang, *Adv. Funct. Mater.* **2024**, *34*, 2411029.
[35] G. Ge, K. Mandal, R. Haghniaz, M. Li, X. Xiao, L. Carlson, V. Jucaud, M. R. Dokmeci, G. W. Ho, A. Khademhosseini, *Adv. Funct. Mater.* **2023**, *33*, 2207388.
[36] Y. Lv, C. Li, Z. Yang, M. Gan, Y. Wang, M. Lu, X. Zhang, L. Min, *Adv. Sci.* **2024**, *11*, 2410446.
[37] C. Xu, A. Xie, H. Hu, Z. Wang, Y. Feng, D. Wang, W. Liu, *Nat. Commun.* **2025**, *16*, 2589.
[38] L. X. Hou, H. Ju, X. P. Hao, H. Zhang, L. Zhang, Z. He, J. Wang, Q. Zheng, Z. L. Wu, *Adv. Mater.* **2023**, *35*, 2300244.
[39] D. Zhang, Y. Liu, Y. Liu, Y. Peng, Y. Tang, L. Xiong, X. Gong, J. Zheng, *Adv. Mater.* **2021**, *33*, 2104006.
[40] S. Wu, Z. Liu, C. Gong, W. Li, S. Xu, R. Wen, W. Feng, Z. Qiu, Y. Yan, *Nat. Commun.* **2024**, *15*, 4441.
[41] H. Wang, Q. Ding, Y. Luo, Z. Wu, J. Yu, H. Chen, Y. Zhou, H. Zhang, K. Tao, X. Chen, J. Fu, J. Wu, *Adv. Mater.* **2024**, *36*, 2309868.
[42] C. Li, J. Liu, X. Qiu, X. Yang, X. Huang, X. Zhang, *Angew. Chem., Int. Ed.* **2023**, *62*, 202313971.